

Photo-crosslinkable Poly(aspartic acid) for Light-based Additive Manufacturing: Chain-growth Versus Step-growth Crosslinking

Lauren De Grave^{a,b}, Celeste Di Meo^c, Coralie Gréant^a, Bo Van Durme^a, Melanie Gérard^d, Annalisa La Gatta^c, Chiara Schiraldi^c, Lieven Thorrez^d, Katrien V. Bernaerts^b, Sandra Van Vlierberghe^{a,*}

^a Polymer Chemistry and Biomaterials Group (PBM), Centre of Macromolecular Chemistry, Department of Organic and Macromolecular Chemistry, Ghent University, Krijgslaan 281, Building S4-bis, 9000 Ghent, Belgium

^b Sustainable Polymer Synthesis group, Aachen-Maastricht Institute for Biobased Materials (AMIBM), Maastricht University, Brightlands Chemelot Campus, Urmonderbaan 22, 6167 RD Geleen, the Netherlands

^c Department of Experimental Medicine, University of Campania “Luigi Vanvitelli”, Via De Crecchio 7, 80138 Naples, Italy

^d Tissue Engineering Lab, Department of Development and Regeneration, KU Leuven, E. Sabbelaan 53, 8500 Kortrijk, Belgium

* Corresponding author: Sandra.VanVlierberghe@UGent.be

Abstract

Crosslinked poly(aspartic acid) (pAsp) hydrogels have been evaluated in various applications benefitting from their biocompatibility and biodegradability. Several crosslinking mechanisms for pAsp derivatives have been investigated, yet research focusing on functionalization of pAsp with photo-crosslinkable moieties is scarce. However, the latter would be beneficial for processing of pAsp through light-based additive manufacturing techniques. pAsp was functionalized comparing two types of photo-crosslinkable moieties (*i.e.* norbornene versus methacrylate), resulting in a thiol-ene step-growth crosslinking mechanism and a chain-growth mechanism, respectively. The influence of the crosslinking mechanism on the photo-crosslinking kinetics, mechanical properties and biocompatibility of the hydrogels was studied. Hydrogels based on norbornene-modified pAsp with Li-TPO-L photo-initiator and a thiol-based crosslinker showed fast crosslinking kinetics and a high swelling ratio, along with a relatively low storage modulus of 29.4 ± 1.3 kPa. Methacrylate-modified pAsp formulations with Li-TPO-L crosslinked slower and exhibited a lower swelling ratio, yet a higher storage modulus (135.1 ± 4.7 kPa). Both hydrogel materials were non-cytotoxic to cells growing in their vicinity. The applicability of the hydrogels to serve as materials for digital light processing (DLP) and two-photon polymerization (2PP) was elucidated. Both materials were processable via DLP and 2PP, offering possibilities towards processing of these materials into constructs serving biomedical applications.

Keywords

Photo-crosslinkable poly(aspartic acid), chain-growth crosslinking, step-growth crosslinking, light-based additive manufacturing, non-cytotoxic hydrogels

1. Introduction

Anionic polyelectrolytes are polymers with acidic moieties in their backbone, rendering them water-soluble, making them interesting candidate materials for a variety of applications [1]. Poly(aspartic acid) (pAsp) is a well-established example of a biodegradable anionic polyelectrolyte with great potential to replace non-degradable anionic counterparts such as poly(acrylic acid). pAsp is a biobased and biocompatible poly(amino acid), that is degradable by specific enzymes and/or microorganisms (*e.g.* activated sludge), hence releasing solely non-toxic compounds [2–4]. pAsp is water-soluble and when crosslinked, it exhibits high water-absorption capacity (up to > 900 times its own weight) [5, 6]. Furthermore, its production is straightforward, since it is synthesized from polysuccinimide (pSI), which in turn is synthesized through polycondensation of aspartic acid or reaction of maleic anhydride with NH_3 or NH_4OH , all commercially available starting materials [7]. Modified pAsp can be obtained via a ring-opening reaction of pSI with primary amines under mild conditions followed by alkaline hydrolysis of the remaining succinimide units [8]. In principle, any primary amine can be used to modify pSI, resulting in a wide range of pAsp derivatives. This versatility combined with its biocompatibility and biodegradability renders modified pAsp a valuable material in the context of biomedical applications (*e.g.* tissue engineering, drug and gene delivery, antifouling coatings and biomineralization) [9–13].

For the above-mentioned purposes, crosslinked pAsp is required, which is generally realized through reaction with diamines [14] or via the formation of disulfide bonds [7]. Diamine crosslinkers with different chain lengths have been described extensively in literature, ranging from hydrazine to long-chain natural polyamines [15–18]. Crosslinking via disulfide bonds occurs through modification of pSI with cysteine or cysteamine, followed by oxidation. An interesting feature of this type of crosslinking, is that the disulfide bonds can be broken again through reduction, making the crosslinking reversible [19, 20]. This reversible crosslinking can be combined with permanent crosslinking, for example with diamines, to maintain structural integrity. This allows to create redox-responsive hydrogels that can change their network density and hence swelling properties under the influence of external triggers [21, 22]. Examples hereof are oxidizing/reducing agents or a change in pH, making these hydrogels interesting for controlled drug delivery and mucoadhesion applications [23–27]. However, reports on photo-crosslinkable pAsp are scarce [28]. Nevertheless, the introduction of photo-crosslinkable moieties in pAsp would allow processing via light-based additive manufacturing (AM) methods, including stereolithography (SLA), digital light processing (DLP) and two-photon polymerization (2PP). Light-based AM techniques are characterized by a high speed and precision as well as excellent computer-aided design and manufacturing (CAD-CAM) mimicry, which is beneficial in the context of biomedical applications (*e.g.* tissue engineering) [29]. Possible photoreactive moieties for light-based AM include, but are not limited to (meth)acrylates, thiols, norbornene and alkenes. By incorporation of these moieties, several photo-crosslinkable natural polymers (*e.g.* based on gelatin [30–33], collagen [34–36], hyaluronic acid [37] and alginate [38–40]) and synthetic polymers (*e.g.* based on polyethylene glycol (PEG) [41, 42] and poly(ϵ -caprolactone) [43]) have been made. Crosslinking of these polymers can be initiated by free radicals resulting from the cleavage of a light-sensitive photo-initiator, forming a crosslinked network with generally a fast curing rate, short exposure time and good reproducibility [44].

Depending on the incorporated functional groups, two main mechanisms for light-induced crosslinking can be distinguished, namely chain-growth and step-growth polymerization [45]. Both mechanisms have been extensively exploited for photo-crosslinking of natural polymers, but crosslinking based on chain-growth polymerization is the most frequently reported for the biopolymers mentioned in the previous paragraph [30, 32, 38, 39]. The mechanism relies on the radical polymerization of (meth)acrylates or (meth)acrylamides, resulting in the formation of oligomer chains, which connect the polymer backbones [30, 46]. Chain-growth polymerization has several benefits, namely easy material handling and no need for an additional crosslinker [29, 44]. Limitations of the mechanism include poor control over reaction kinetics and the formation of a heterogeneously crosslinked network, as not all initiated radicals will undergo the same number of propagation steps prior to termination [47, 48]. Furthermore, the reaction is sensitive to oxygen inhibition and unreacted double bonds remain present after crosslinking [49]. Step-growth crosslinking can occur between two compounds bearing complementary functional groups [50]. In the latter regard, “click” chemistry has gained increasing attention. “Click” reactions are fast, provide excellent control and high yields, are wide in scope and are not sensitive to oxygen inhibition or side reactions with water [51]. The most common step-growth mechanism for crosslinking of biopolymers is thiol-ene (photo-)click chemistry. This mechanism involves a reaction of a thiol with an ene-functionality, e.g. norbornene, vinyl ethers, (meth)acrylates, styrene, (meth)acrylamides and conjugated dienes, initiated by a radical initiator [52]. Any type of non-sterically hindered double bonds is a potential ene-functionality, but superior control over the step-growth polymerization can be obtained if the ene-function cannot undergo a competitive chain-growth polymerization, rendering for example (meth)acrylates and (meth)acrylamides less suitable [53]. In addition, since the crosslinking rate is determined by the chain transfer step, the reaction will be slower when the radical is stabilized by mesomeric stabilization, which is the case for methacrylates, styrene and conjugated dienes. The thiol-norbornene reaction is widely used for the crosslinking of biopolymers since the reaction is very fast due to the relief of ring strain upon thiol-carbon bond formation [54]. Other benefits of thiol-ene step-growth crosslinking include the formation of a more homogeneous network, high functional group conversion (> 99%), fast reaction rates and no susceptibility to oxygen inhibition [52, 55]. However, disadvantages involve the need to incorporate a multifunctional crosslinker which can participate in side reactions and the formation of hydrogels with a lower storage modulus compared to chain-growth crosslinked hydrogels [56–58].

We herein report the modification of pAsp with photo-crosslinkable moieties and compare crosslinking via a chain-growth versus step-growth polymerization mechanism, which is unprecedented for pAsp. pAsp was modified with two types of photo-crosslinkable functionalities (*i.e.* norbornene and methacrylate) and their crosslinking kinetics were studied via *in situ* photo-rheology. Hydrogels of both pAsp derivatives were developed and their swelling degree and gel fraction were studied. Our data show that both norbornene and methacrylate give rise to fast photo-crosslinking, offering unprecedented processing possibilities for pAsp. Furthermore, an *in vitro* cell viability assay was performed to determine the cytotoxicity and the impact of the developed materials on cell viability. Finally, we provided a first proof-of-concept towards processing of pAsp via two light-based printing techniques, namely DLP and 2PP.

2. Materials and methods

2.1. Materials

All chemicals were used as received unless stated otherwise. *N,N*-dimethylformamide (DMF, > 99.9%) was purchased from VWR. Sodium hydroxide (NaOH, pellets), *DL*-dithiothreitol (DTT, 97%), triethylamine (TEA, ≥ 99%), hydrochloric acid (HCl, 37%), 4-*tert*-butylcatechol (TBC), phosphate buffered saline (PBS, tablets) and tartrazine (dye content ≥ 85%) were purchased from Sigma-Aldrich. 5-Norbornene-2-methylamine (mixture of isomers, > 98%) was acquired from TCI Europe. 2-Aminoethyl methacrylate hydrochloride (AEMA.HCl, ≥ 95%) was obtained from Polysciences Europe. Methanol (MeOH, >99%) was purchased from Chem-Lab. Ethyl acetate was supplied by UnivarSolutions. Dimethylsulfoxide (DMSO, 99.7%) was purchased from Thermo Scientific and distilled before use. Deuterated dimethylsulfoxide (*d*6-DMSO, 99.8% D) and deuterium oxide (D₂O, 99.9% D) were obtained from Eurisotop. Polysuccinimide (pSI) was prepared according to a previously described procedure [28]. Lithium (2,4,6-trimethylbenzoyl)phenylphosphinate (Li-TPO-L) was prepared according to a procedure reported by Markovic *et al.* [59]. Dialysis membranes (Spectra/Por MWCO 3500 g mol⁻¹) were purchased from Polylab. Double distilled water (DDW) was used for the preparation of aqueous solutions and to perform swelling experiments (Merck Synergy UV, Millipore Milli-Q gradient, $\rho = 18.2 \text{ M}\Omega \text{ cm}$ at 25 °C).

2.2. Synthesis of photo-crosslinkable poly(aspartic acid) derivatives

Norbornene-modified poly(aspartic acid) (pAsp-NB) was obtained by modification of pSI with 5-norbornene-2-methylamine (NB-NH₂), followed by hydrolysis of the intermediate and dialysis. 20.00 g pSI (0.21 mol succinimide units ($M = 97.07 \text{ g mol}^{-1}$)) was dissolved in 200 mL DMF in a flame-dried two-neck flask while stirring and heating to 60 °C. After complete dissolution, 5.07 mL NB-NH₂ (0.20 eq. relative to the succinimide units, 0.040 mol, 5.07 g) was added to the pSI solution. The system was filled with argon gas and degassed 3 times, afterwards the reaction was continued for 24 h at 60 °C. The polymer was precipitated by addition of the reaction solution to 2000 mL ethyl acetate, followed by filtration. The precipitate was washed 3 times with ethyl acetate and dried under reduced pressure at 50 °C for 48 h to obtain norbornene-modified pSI (pSI-NB) as intermediate product. pSI-NB was dispersed in DDW at a concentration of 10 w/v%. The pH was adjusted to 10 by adding aqueous NaOH (1 M) dropwise to the suspension in order to hydrolyze the succinimide units. The suspension was stirred for 3 h while regularly checking the pH and readjusting to pH 10 if necessary, until the polymer dissolved. The solution was dialyzed against DDW (Spectra/Por MWCO 3500 g mol⁻¹) for 24 h with the water being changed 6 times. Finally, pAsp-NB was obtained after freezing and lyophilization (Christ freeze-dryer Alpha 2-4 LSC) as white/yellow fine powder (90% yield).

For the synthesis of aminoethyl methacrylate-modified poly(aspartic acid) (pAsp-AEMA), 30.00 g pSI (0.31 mol succinimide units ($M = 97.07 \text{ g mol}^{-1}$)) was dissolved in 200 mL distilled DMSO, in a flame-dried two-neck flask while stirring and heating to 60 °C. 12.80 g AEMA.HCl (0.25 eq. relative to the succinimide units, 0.077 mol) and 0.13 g TBC (0.0025 eq. relative to the succinimide units, 0.77 mmol) were dissolved in a separate round-bottom flask in 100 mL distilled DMSO, while stirring and heating to 60 °C. The solution was shielded from light to prevent polymerization. After complete dissolution, 11.85 mL TEA (0.28 eq. relative to the succinimide units, 0.085 mol, 8.60 g) was added to the AEMA.HCl

solution. Afterwards, the AEMA.HCl solution was added dropwise to the pSI solution. After complete addition, the system was filled with argon and degassed 3 times. The reaction was shielded from light and continued for 24 h at 60 °C. The solution was added dropwise to 3000 mL HCl solution (0.50 M) to neutralize the excess base and to precipitate the polymer. The precipitate was filtered and washed 2 times with DDW and 2 times with MeOH. The precipitate was dried under reduced pressure at 50 °C for 48 h to obtain AEMA-modified pSI (pSI-AEMA) as intermediate product. pSI-AEMA was dispersed in DDW at a concentration of 10 w/v%. The pH was adjusted to 10 by adding aqueous NaOH (1 M) dropwise to the suspension in order to hydrolyze the remaining succinimide units. The reaction mixture was stirred for 3 h while regularly checking the pH and readjusting to pH 10 if necessary. The solution was dialyzed against DDW (Spectra/Por MWCO 3500 g mol⁻¹) for 24 h with the water being changed 5 times. Finally, pAsp-AEMA was obtained after freezing and lyophilization as fine white powder (87% yield).

2.3. Polymer characterization

2.3.1. Nuclear magnetic resonance (¹H-NMR) spectroscopy

¹H-NMR spectra were recorded on a 300 MHz Bruker Avance I Ultrashield spectrometer at room temperature with *d*6-DMSO or D₂O as solvent. Spectra were analyzed using MestReNova software.

2.3.2. Gel permeation chromatography (GPC)

Gel permeation chromatography (GPC) measurements in DMF were performed on a Waters Alliance e2696 Separations Module device coupled to one Styragel Guard Column (4.6 x 30 mm, 20 μm particle size) and three Styragel GPC Columns (7.8 x 300 mm, 5 μm particle size) with variable molecular weight range (*M_w*) of 0 – 1000 g mol⁻¹, 500 – 20000 g mol⁻¹ and 5000 – 600000 g mol⁻¹ connected in sequence with a column temperature of 40 °C. Detection was based on a refractive index (RI) detector 2414 with RID temperature 35 °C. Molar masses were determined from the obtained retention times via an external calibration curve using ReadyCal-Kit PMMA standards (*M_p* = 800 – 2200000 g mol⁻¹). As eluent DMF + 0.035 mol L⁻¹ LiCl + 6 mol L⁻¹ glacial acetic acid was used at a flow rate of 1 mL min⁻¹. Samples were prepared by dissolving 2 – 5 mg of polymer in 1.5 mL of eluent.

Aqueous GPC measurements were performed using a Waters 600 controller connected to a Waters 410 differential refractometer detector to determine the molar mass and dispersity. Injection was done using a Waters 610 Fluid Unit. One Guard Column (Shodex OHpak SB-G 6B, 6.0 x 50 mm, 10 μm particle size) and two columns for aqueous SEC (Shodex OHpak SB-806M HQ, 8.0 x 300 mm, 13 μm particle size) with a molecular weight range (*M_w*) of 500 – 20000000 g mol⁻¹ were connected in sequence. Molar masses were determined from the obtained retention times via an external calibration curve with a set of pullulan standards from Shodex (*M_p* = 6100, 21100, 47100 and 107000 g mol⁻¹). A phosphate buffer (Na₂HPO₄/NaH₂PO₄, pH 7, 0.1 M) was used as eluent at a flow rate of 1 mL min⁻¹. Samples were prepared by dissolving 10 mg polymer in 1 mL eluent. Samples were filtered over hydrophobic PTFE syringe filters with pore size 0.45 μm before injection. Spectra were analyzed using Waters Empower2 software.

2.3.3. Photo-rheology

Photo-rheology measurements were carried out on an Anton Paar MCR 302e rheometer with parallel plate-plate geometry, with an upper plate diameter of 25 mm. All measurements were performed at 21 °C with an oscillatory frequency of 1 Hz, a strain of 0.1% and a measuring gap of 0.30 mm. 300 μ L of the sample was injected between the parallel plates, the samples were trimmed and irradiated through a glass bottom plate using UV-A light with a wavelength of 365 nm and an intensity of 100 mW cm⁻² (OmniCure series 1500 UV light source). The samples were not irradiated with UV light during the first 60 s to allow them to settle following handling, after which the samples were irradiated during 600 s to induce curing. After 600 s, the UV light was switched off and potential post-curing was monitored during 240 s [60]. Solutions with a concentration of 30 w/v% pAsp-NB or pAsp-AEMA in DDW containing 2 mol% Li-TPO-L, relative to the number of crosslinkable functionalities present in the polymer, were used. For pAsp-NB, 0.50 eq. DTT, relative to the number of norbornene functionalities, was added as crosslinker corresponding to an equimolar thiol-ene ratio. Measurements were executed three times to indicate reproducibility.

2.4. Hydrogel preparation and characterization

2.4.1. Crosslinking of hydrogel sheets via film casting

For the preparation of crosslinked hydrogels, precursor solutions with the same composition as used in the photo-rheology measurements were prepared. Each solution was injected between two parallel glass plates with Teflon release foil and a silicone spacer of 1 mm thickness. The plates were irradiated for 30 min on both sides with UV-A light (365 nm, UVP High Performance UV Transilluminator) with an intensity of 10 mW cm⁻² to induce crosslinking of the precursor solution. After irradiation, the plates were removed from each other to obtain the crosslinked hydrogel sheet.

2.4.2. Swelling and gel fraction studies

For determination of the swelling ratio and gel fraction, circular samples ($\varnothing = 8$ mm) were punched out of the hydrogel sheets. The circular samples were frozen and lyophilized to determine the initial dry mass. The samples were incubated in DDW for 3 days at 20 °C. Afterwards, the samples were removed from DDW, the surface was gently dried and the samples were weighted to determine the swollen mass. Then, the samples were frozen again and lyophilized to determine the final dry mass. The mass swelling ratio and gel fraction were calculated according to equations (1) and (2), respectively:

$$\text{Mass swelling ratio} = \frac{m_s - m_{d,2}}{m_{d,2}} \quad (1)$$

$$\text{Gel fraction (GF)} = \frac{m_{d,2}}{m_{d,1}} \times 100 \% \quad (2)$$

$m_{d,1}$ is the initial freeze-dried mass of the sample before swelling, $m_{d,2}$ is the final freeze-dried mass of the sample after swelling and m_s is the mass of the sample in swollen state. All measurements were performed in triplicate for statistical relevance.

2.5. Quantification of cell metabolic activity via Alamar Blue assay

Before the assay, circular hydrogel films ($\varnothing = 20$ mm) were sterilized by incubation for 24 h in 70% ethanol (EtOH), incorporating 3 EtOH washing steps. The films were exposed to UV-C light (254 nm) for 30 min in a final sterilization step. Thereafter, they were hydrated in PBS for 72 h, including 3 PBS washing steps. HEK 293T cells were thawed and cultured at 37 °C in a 5% CO₂ environment in growth medium (DMEM high glucose w/glutamine w/sodium pyruvate (Biowest) containing 10% fetal bovine serum and 1% penicillin/streptomycin solution (Avantor)). After reaching confluency, the cells were plated in a 6-well plate at 500000 cells per well. In each well, a cell strainer (Corning, 100 μ m pore size) was placed containing one sterilized and hydrated hydrogel film. The medium volume was increased to submerge the hydrogels in the growth medium of the cells. The cells were incubated at 37 °C and 5% CO₂ for 24 h, followed by the start of Alamar Blue assay. The cell strainers were temporarily removed from the 6-well plate and the medium was replaced by Alamar Blue solution (44 μ M resazurin sodium salt (Merck) in Hanks Balanced Salt Solution (HBSS, ThermoFisher Scientific)). Cells were incubated with equal volumes of the Alamar Blue solution at 37 °C and 5% CO₂ for 1 h, after which a 200 μ L sample was pipetted in a white, flat bottom 96-well plate (ThermoFisher Scientific). The remainder of the Alamar Blue solution on the cells was replaced by growth medium, the cell strainers with the hydrogel were replaced in the well plates and the cells were incubated for another 24 h. The Alamar Blue assay was performed every 24 h for 4 days. In between sampling times, the white 96-well plate containing the Alamar Blue solution samples was stored in the dark at 4 °C. Finally, resazurin fluorescence in the samples was measured at 580-640 nm (excitation 525 nm) to determine cell metabolic activity (GloMax Multi fluorescence plate reader, Promega).

2.6. Light-based additive manufacturing

2.6.1. Digital light processing (DLP)

To obtain resins that could be printed by DLP, 40 w/v% pAsp-AEMA and 20 w/v% pAsp-NB solutions were prepared. The polymer concentrations were chosen to obtain a well-dissolved solution with a suitable viscosity (< 3 Pa s at 100 s⁻¹ shear rate and 25 °C) [61]. Photo-rheology measurements were done to determine the optimal photo-initiator (PI) and photo-absorber (PA) concentration for both formulations. The Li-TPO-L concentration was varied between 0.5 and 40 mol% (relative to the number of crosslinkable functionalities present) and the tartrazine concentration (PA) between 0.5 and 2 mol%. Eventually, 10 mol% Li-TPO-L and 1 mol% tartrazine versus 0.5 mol% Li-TPO-L and 1 mol% tartrazine were added to pAsp-AEMA and pAsp-NB, respectively. Moreover, 0.50 eq. DTT was added to pAsp-NB. These resins were processed using a LumenX DLP printer from Cellink, equipped with a 405 nm LED and a digital micromirror device. The build platform offset was set to 0 and a temperature of 37 °C was fixed for each printing session. A CAD design of the "Pisa Tower" with dimensions 30 x 10.8 x 10.8 mm³ was used for DLP with a resin volume of 3.45 mL. To optimize the parameters of the printer in terms of UV light exposure and time of irradiation, the working curve was derived for both hydrogels by assessing the thickness of a cured monolayer, obtained at different cure doses. Particularly, a square of 1 cm² was printed on glass slides without any build platform, using a constant intensity of 23.16 mW cm⁻² (50% of the maximal intensity of the DLP) and an exposure time ranging from 4 to 14 s [43]. The layer obtained was placed between two glass slides and the thickness was evaluated with a Zeiss

Axiotech 100 HD light microscope [62]. To ensure the reproducibility, each cure dose was tested at least in triplicate for both solutions. The minimal energy required for polymerization (E_c) and the penetration depth of the curing light (D_p) were calculated according to Jacobs' equation (3):

$$C_d = D_p \ln \frac{E}{E_c} \quad (3)$$

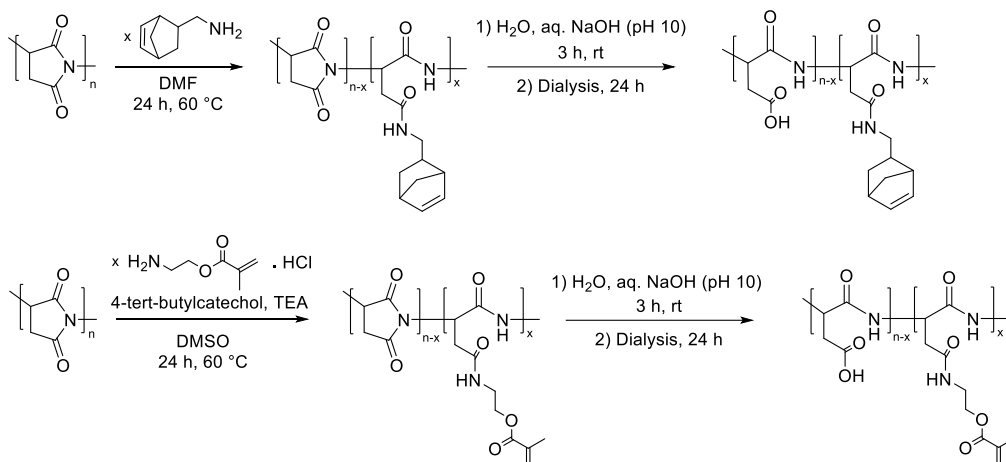
where C_d and E represent the thickness of the cured resin and the applied energy dose, respectively [63].

2.6.2. Two-photon polymerization (2PP)

Two-photon polymerization was performed using a NanoOne Bio high-resolution 3D printer from UpNano GmbH equipped with a 10x air immersion objective (NA 0.4, WD 3.10 mm, Zeiss) and a variable microscope-stage insert. The device was equipped with a femtosecond fiber laser with 90 fs pulse length, 80 MHz repetition rate, 780 nm center wavelength and maximal average laser power of 1000 mW. Precursor solutions of 30 w/v% pAsp-AEMA or pAsp-NB in PBS containing 1 mM sodium 3,3'-((((1E,1'E)-(2-oxocyclopentane-1,3-diyliidene)bis(methanylylidene))bis(4,1-phenylene))bis(methylazanediy))dipropanoate (P2CK) as two-photon initiator were employed [64]. For pAsp-NB, 0.50 eq. DTT was added to the precursor solution. 100 μ L of the solution was added onto a microscope slide silanized with 3-(trimethoxysilyl)propyl methacrylate to ensure attachment of the printed structures during sample development. The optimal 2PP threshold laser power was determined by printing 100 x 100 x 100 μ m³ cubes at a constant scanning speed of 600 mm s⁻¹ and for varying laser powers. For pAsp-AEMA, average laser powers were varied from 100 to 250 mW with increments of 10 mW. For pAsp-NB, average laser powers were varied from 5 to 100 mW with increments of 5 mW. The average laser powers and increments were selected based on previous reports focusing on photo-crosslinkable gelatins processed via 2PP [31]. Afterwards, a CAD design of a snowflake ($x = 200 \mu$ m, $y = 180 \mu$ m and $z = 100 \mu$ m) was printed with the optimal scanning speed and laser power as determined by the 2PP structuring performance test. The CAD design was sliced with 5 μ m layer spacing (Δz) and hatched with 0.50 μ m line spacing (Δxy). Sample development was done by adding 10 mL PBS in a petri dish followed by immersion of the sample for 6 h at room temperature to allow complete dissolution of the non-crosslinked material. Samples were studied with a Zeiss Axiotech 100 HD light microscope and a Zeiss LSM 710 laser scanning confocal microscope. Samples were swollen in PBS before microscopic analysis. Microscope images were analyzed using ImageJ software.

3. Results and discussion

3.1. Synthesis and characterization of photo-crosslinkable poly(aspartic acid) derivatives



Scheme 1. Reaction scheme for the synthesis of pAsp-NB (top) and pAsp-AEMA (bottom) by modification of pSI with x equivalents of the respective primary amine followed by hydrolysis and dialysis.

Two types of photo-crosslinkable pAsp-derivatives were synthesized through modification of a pSI ($M_n = 16900 \text{ g mol}^{-1}$, $M_w = 36600 \text{ g mol}^{-1}$, $M_z = 54800 \text{ g mol}^{-1}$, $\bar{D} = 2.2$ as determined via GPC in DMF) precursor with a functional primary amine, followed by alkaline hydrolysis and dialysis (**Scheme 1**). pAsp-NB was synthesized through reaction of pSI with 0.20 eq. (relative to the succinimide units) NB-NH₂, resulting in pSI-NB as intermediate. pAsp-NB was obtained by ring-opening of the succinimide units in the intermediate through alkaline hydrolysis (pH 10) for 3 h. The product was purified via dialysis for 24 h, followed by lyophilization to yield pAsp-NB ($M_n = 4600 \text{ g mol}^{-1}$ and $\bar{D} = 1.5$ as obtained via aqueous GPC) as white/yellow fine powder with an overall yield of 90%. The GPC chromatogram is provided in the supplementary information (SI) (**Figure S1**). The degree of substitution (DS) was calculated based on the relative integrations obtained from ¹H-NMR spectra of the pSI-NB intermediate, resulting in a DS of 18% (**Figure S3, SI**). The ratio of closed succinimide units, opened aspartic acid units and NB-modified aspartic acid units was calculated through the relative integrations of the characteristic signals obtained from the ¹H-NMR spectra of pAsp-NB (**Figure S5, SI**).

For the synthesis of pAsp-AEMA, pSI ($M_n = 26000 \text{ g mol}^{-1}$, $M_w = 67700 \text{ g mol}^{-1}$, $M_z = 112800 \text{ g mol}^{-1}$, $\bar{D} = 2.6$ as determined via GPC in DMF) was reacted with 0.25 eq. AEMA.HCl (relative to the succinimide units). TEA was added to activate the primary amine to enable nucleophilic attack on the carbonyl moieties, while TBC was added to prevent premature polymerization of the methacrylate moieties. The obtained pSI-AEMA was hydrolyzed by addition of aqueous NaOH (pH 10) for 3 h to obtain pAsp-AEMA. After purification through dialysis and lyophilization, the product was obtained with an overall yield of 72%, while the aqueous GPC data indicated $M_n = 13100 \text{ g mol}^{-1}$ and $\bar{D} = 2.0$. The GPC chromatogram is included in the Supplementary information (**Figure S2**). The DS was again calculated through the relative integrations of the characteristic peaks obtained from the ¹H-NMR spectra, resulting in a DS of 8% (**Figure S4, SI**). The ratio of closed succinimide units, opened aspartic acid units and AEMA-

modified aspartic acid units was calculated via the relative integrations of the characteristic signals obtained from the $^1\text{H-NMR}$ spectra of pAsp-AEMA (**Figure S6, SI**).

The crosslinking ability and kinetics were studied by *in situ* photo-rheology measurements. To study the evolution in storage (G') and loss moduli (G''), formulations of 30 w/v% pAsp-NB and pAsp-AEMA were made in DDW containing 2 mol% Li-TPO-L, as well as 0.50 eq. DTT in case of pAsp-NB. The concentration of DTT was chosen to ensure an equimolar ratio between thiol and norbornene functionalities present in pAsp-NB. The evolution in G' and G'' upon UV-A irradiation with a light intensity of 100 mW cm^{-2} was monitored as a function of time (**Figure 1**). G'' was higher than G' for both formulations before the UV light was turned on, indicating that the formulations are liquid prior to irradiation. After 60 s of stabilization time, UV irradiation was initiated, resulting in an immediate and steep increase of G' for both formulations and a cross-over between G' and G'' . This cross-over point is defined as the gel point and marks the moment when the behavior of the formulation goes from a dominantly liquid character to a dominantly elastic character, due to the transition from liquid to gel upon crosslinking [65]. The gel point was 1.5 s for pAsp-NB and 2.5 s for pAsp-AEMA, indicating slightly faster crosslinking in case of thiol-ene step-growth crosslinking as compared to methacrylate chain-growth crosslinking. For pAsp-NB, crosslinking occurs via a UV-mediated thiol-ene reaction occurring between a norbornene function of pAsp-NB and a thiol function of DTT. Because DTT is a bifunctional thiol, it acts as a crosslinker since one thiol function only reacts with one norbornene functionality, connecting two pAsp-NB chains to each other [31]. pAsp-AEMA, on the other hand, crosslinks via an UV-induced chain-growth mechanism during which a radical is created on a methacrylate function, which can propagate by attacking another methacrylate function. In this way, two or more pAsp-AEMA chains are attached to each other via a chain-growth mechanism until the propagating radical is terminated by recombination or disproportionation [32]. After a few seconds of UV irradiation, the slope of G' gradually decreased evidencing reduced crosslinking kinetics when the network became more dense and the concentration of functional groups reduced. The slope decreased more gradually for pAsp-AEMA, which is inherent to the chain-growth mechanism, compared to a more abrupt change in slope in case of pAsp-NB, as reported earlier for other hydrogel types [30]. The chain-growth mechanism is characterized by a delay upon UV irradiation as a result of oxygen inhibition. Before the initiated radicals can start polymerizing, they will first consume the oxygen present. This is not the case for thiol-ene step-growth crosslinking, resulting in a faster crosslinking and hence, the steeper slope observed [66]. After a few seconds, a plateau value was reached for G' which remained constant following UV irradiation. This post-polymerization G' was higher for pAsp-AEMA compared to pAsp-NB. For pAsp-AEMA, a final G' of $135.1 \pm 4.7 \text{ kPa}$ was obtained, while G' was $29.4 \pm 1.3 \text{ kPa}$ for pAsp-NB. G' is a measure for the stiffness of a network, as a stiffer network has a higher elastic response, resulting in a higher G' [67]. Hence, step-growth crosslinking resulted in a lower post-polymerization G' and thus in hydrogels with a lower mechanical stiffness compared to hydrogels formed via chain-growth crosslinking, due to the absence of kinetic chains in case of thiol-NB crosslinking. These results are in agreement with previous reports in literature for poly(ϵ -caprolactone) and gelatin-based hydrogels [30, 43, 67].

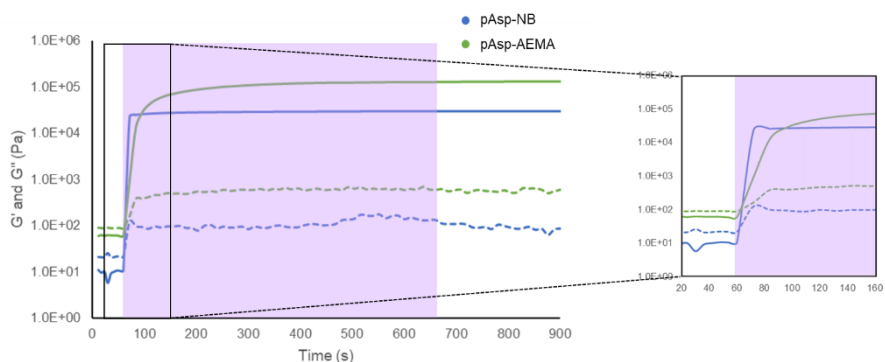


Figure 1. Photo-rheological monitoring of the evolution in storage (solid lines) and loss moduli (dashed lines) of 30 w/v% solutions of pAsp-NB and pAsp-AEMA containing 2 mol% Li-TPO-L (and 0.50 eq. DTT for pAsp-NB) upon UV-A irradiation (100 mW cm^{-2}). On the right, a magnification of the behavior of storage and loss moduli during the first increment of irradiation is shown, as well as the gel points for both materials.

3.2. Hydrogel formation and swelling experiments

Hydrogels of pAsp-NB and pAsp-AEMA were created by film casting. The standard composition of the formulations was a 30 w/v% solution in DDW containing 2 mol% Li-TPO-L and 0.50 eq. DTT in case of pAsp-NB. Furthermore, Li-TPO-L concentrations of 4 and 8 mol% were used in combination with 30 w/v% pAsp-AEMA and for 30 w/v% pAsp-NB, the Li-TPO-L concentration was varied between 2 and 4 mol% in combination with 0.50 or 1 eq. DTT. After film casting, circular samples were punched out and dried by lyophilization. Swelling and gel fraction experiments were performed on the circular samples to determine the network integrity and to gain more insight in the effect of the crosslinking mechanism on the network topology [68]. The obtained results are summarized in **Table 1**.

For the hydrogels prepared with the standard formulation, gel fractions of $75.9 \pm 2.8\%$ and $87.8 \pm 4.2\%$ were obtained for pAsp-NB and pAsp-AEMA respectively. The higher gel fraction observed for pAsp-AEMA compared to pAsp-NB indicates a more efficient network formation and a lower presence of non-crosslinked species that leached out during the experiment in case of pAsp-AEMA. The recorded mass swelling ratio of the circular samples from the standard formulations following 3 days incubation in DDW was $7.4 \pm 0.2 \text{ g g}^{-1}$ for pAsp-AEMA and $45.7 \pm 2.0 \text{ g g}^{-1}$ for pAsp-NB. The lower swelling ratio for pAsp-AEMA was not anticipated considering the structural differences of the polymers, since pAsp-AEMA contains a higher aspartic acid/succinimide ratio compared to pAsp-NB, which would result in higher swelling for pAsp-AEMA networks (Table S1 and S2, SI). However, the difference in swelling ratio can be explained taking into account the difference in gel fraction, network density and network topology. First, the lower swelling ratio for pAsp-AEMA is a result of the higher gel fraction observed, resulting in the formation of a denser network. On the other hand, the higher network density is also a consequence of the formation of kinetic chains upon crosslinking of pAsp-AEMA [67]. Finally, the swelling ratio is also influenced by the network topology, as a homogeneous network generally results in a higher swelling ratio compared to a heterogeneous network [43]. Hence, the higher swelling ratio for pAsp-NB can also be attributed to the more homogeneous topology when comparing thiol-ene step-growth crosslinking to methacrylate chain-growth crosslinking. In case of thiol-ene crosslinking, the reaction is orthogonal since one thiol reacts with one norbornene functionality, linking two chains to each other [55]. The network

density will therefore mainly depend on the number of functionalities the crosslinker encompasses (e.g. a trifunctional thiol results in a more dense network compared to a similar bifunctional thiol) as well as the chain length of the crosslinker. On the other hand, for chain-growth crosslinking, multiple methacrylate functionalities react with each other resulting in the formation of short hydrophobic oligomeric methacrylate chains. Furthermore, methacrylate functionalities on the same chain can also react with each other, resulting in cyclic chains and network imperfections, which also contribute to the network heterogeneity [66].

For pAsp-AEMA, formulations with photo-initiator concentrations of 4 and 8 mol% were also used in the film casting process. This resulted in the formation of hydrogels exhibiting higher gel fractions of $99.2 \pm 0.8\%$ and $97.8 \pm 2.6\%$, respectively. The higher gel fractions observed upon exploiting higher photo-initiator concentrations indicate a more efficient network formation, with a maximal efficiency for a formulation containing 4 mol% Li-TPO-L. Moreover, the mass swelling ratio slightly increased to $8.3 \pm 0.1 \text{ g g}^{-1}$ and $9.4 \pm 0.2 \text{ g g}^{-1}$, respectively. The trend observed in the swelling ratio relative to the gel fraction and the photo-initiator concentration can be explained by two counterbalancing effects. On the one hand, a higher gel fraction implies the formation of a more densely crosslinked network, which results in a lower swelling ratio. On the other hand, swelling is also governed by the presence of hydrophilic chains, namely pAsp. Hence, a lower gel fraction implies the presence of less hydrophilic chains, which consequently results in a lower swelling ratio. For pAsp-NB, the gel fraction also increases with an increasing Li-TPO-L concentration when comparing a concentration of 2 mol% and 4 mol% in combination with 0.50 eq. DTT. For the last formulation, a gel fraction of $85.4 \pm 4.1\%$ was observed, again indicating more efficient network formation and the presence of less non-crosslinked material compared to the formulation containing 2 mol% Li-TPO-L. When increasing the Li-TPO-L concentration from 2 mol% to 4 mol%, more radicals are initially formed, increasing the efficiency of network formation and the chance for norbornene to react with a thiol resulting in a more densely crosslinked network being formed [52]. Furthermore, the mass swelling ratio decreased to $29.4 \pm 0.4 \text{ g g}^{-1}$, which can also be attributed to the higher network density. For the formulation containing 2 mol% Li-TPO-L in the presence of 1 eq. DTT (so deviating from equimolarity between thiol and NB), hydrogels with a gel fraction of $92.9 \pm 5.6\%$ and mass swelling ratio of $20.1 \pm 2.2 \text{ g g}^{-1}$ were obtained. When 0.50 eq. DTT is used, an equimolar ratio of thiol and NB functionalities is present and since the thiol-ene reaction is orthogonal, one would expect that every NB function reacts with one thiol function. However, some thiol functions will form disulfide bonds with each other, resulting in a deficiency of thiol functions for the thiol-ene reaction to occur, leaving behind unreacted NB functions. By increasing the amount of DTT to 1 eq., an excess of thiol functions is present and the chance for a NB function to encounter a thiol to react with will increase, resulting in a higher efficiency of network formation and a more densely crosslinked network, which explains the lower swelling ratio observed. The data observed are in agreement with previous reports describing thiol-norbornene crosslinked gelatins [31, 69].

Table 1. Gel fraction and mass swelling ratio of hydrogels consisting of 30 w/v% pAsp-AEMA crosslinked with different photo-initiator (PI) concentrations and hydrogels consisting of 30 w/v% pAsp-NB crosslinked with different PI and crosslinker concentrations. The composition of the standard formulation is indicated with an asterisk (*).

pAsp-AEMA	pAsp-NB
-----------	---------

PI concentration (mol%)	Gel fraction (%)	Mass swelling ratio (g g ⁻¹)	PI concentration (mol%)	Crosslinker concentration (eq.)	Gel fraction (%)	Mass swelling ratio (g g ⁻¹)
2*	87.8 ± 4.2*	7.4 ± 0.2*	2*	0.50*	75.9 ± 2.8*	45.7 ± 2.0*
4	99.2 ± 0.8	8.3 ± 0.1	2	1	92.9 ± 5.6	20.1 ± 2.2
8	97.8 ± 2.6	9.4 ± 0.2	4	0.50	85.4 ± 4.1	29.4 ± 0.4

3.3. Cell metabolic activity

Several potential applications of pAsp-based hydrogels, such as tissue engineering and drug delivery, are based on the contact with living cells. Therefore, it is important to confirm that the hydrogel functionalization does not negatively impact cell viability. As a model system, Human Embryonic Kidney cells were chosen. The metabolic activity of cells is a more sensitive marker of the health of cells compared to e.g. cell death markers. Therefore, the Alamar Blue assay was selected to determine if the hydrogels showed cytotoxicity. This assay is based on the principle that viable cells are able to process resazurin salt into resorufin, which is a fluorescent compound. A higher resorufin fluorescence indicates an increased presence of viable cells. In the current setup, an indirect assay was chosen in which no direct contact between the cells and the hydrogels occurs. **Figure 2** shows that both pAsp-NB and pAsp-AEMA allowed normal cell growth and metabolism as seen by the increase in fluorescence over time, which was not statistically different with cells growing in the absence of a hydrogel. However, for the pAsp-AEMA hydrogel, a trend towards cytotoxicity can be observed at later time points which is indicated by the larger deviation in metabolic activity compared to the control condition. It should be noted that, also at those time points, the differences are not statistically significant. These results confirm that the hydrogels do not constitute compounds having a negative influence on the metabolic activity of cells at toxic concentrations that leached out from the hydrogel.

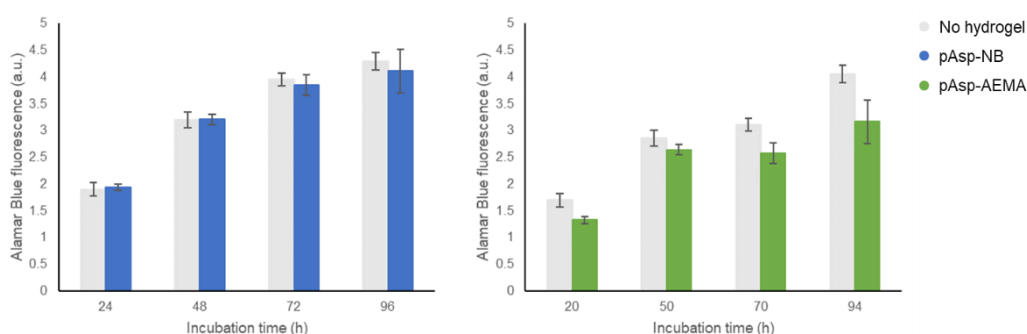


Figure 2. Determination of metabolic activity of HEK 293T cells growing in the vicinity of the hydrogels at various incubation times by an Alamar Blue assay (indirect assay). Alamar Blue fluorescence of cells growing in the vicinity of pAsp-NB (blue) and pAsp-AEMA (green) hydrogels are compared to cells growing in the absence of a hydrogel (grey).

3.4. Processing via DLP and 2PP

3.4.1. DLP

DLP is a 3D printing technology based on the local photo-polymerization of a photocurable resin induced by UV irradiation. It offers efficient printing since it converts 2D images (CAD design) into 3D structures by projecting UV light on an entire layer at once. The nozzle-free system and the opportunity to print in

aqueous solution makes DLP printing ideally suitable for biopolymer-based resins [70]. However, the processability of a material by DLP depends on many factors, such as the viscosity of the resin, the crosslinking ability, the curing kinetics of the biopolymer and the printer settings. To this end, a Jacobs' working curve is commonly exploited, since this provides two parameters of photocurable resins which are essential for the success of the DLP printing process, namely the penetration depth of the curing light and the critical energy dose required for polymerization [63].

The working curves for pAsp-AEMA and pAsp-NB were derived and are reported in **Figure 3a**. Through extrapolation of the linear fitting curves, values of 258 μm and 89 μm were obtained for the penetration depth (D_p) and a critical curing dose E_c of 76 and 24 mJ cm^{-2} was calculated for the pAsp-AEMA and pAsp-NB resins, respectively. These values were determined as the slope of the linear regression (D_p) and the interception of the Jacobs' working curve with the x-axis (E_c), and were within the range for commercial resins established by Bennet *et al.* [62]. The correlation coefficients (R^2) of the logarithmic regression lines were 0.94 for pAsp-AEMA and 0.93 for pAsp-NB. Small deviations in linearity might be justified by errors in the handling of soft cured films and in the calculation of the film thickness [71].

The results illustrate that the sample based on pAsp-NB required an energy for crosslinking which was 3 times lower than for pAsp-AEMA and low irradiation intensities (23.16 mW cm^{-2}) were needed for building the "Pisa Tower" structure with both materials (**Figure 3b**). Since the printing process was expected to succeed when $C_d > z$ where z represents the height of the single layer [71], a layer thickness of 50 μm was chosen as operation parameter. Both resins gave rise to acceptable 3D structures in the working conditions set, although the structure produced with the pAsp-AEMA resin showed a superior CAD-CAM mimicry compared to pAsp-NB, for which overcuring was observed in the upper region of the structure. However, the structure printed with pAsp-AEMA shows more shrinkage compared to the structure constituting pAsp-NB. This is a result of the difference in crosslinking mechanism, as chain-growth crosslinking results in the formation of kinetic chains which makes the resulting hydrogel more susceptible to shrinkage [30]. For chain-growth crosslinking, oligomeric methacrylate chains with variable lengths are formed, resulting in the pAsp-AEMA chains being on average closer together, while for the thiol-ene crosslinking, the thiol crosslinker acts as a spacer between the polymer chains.

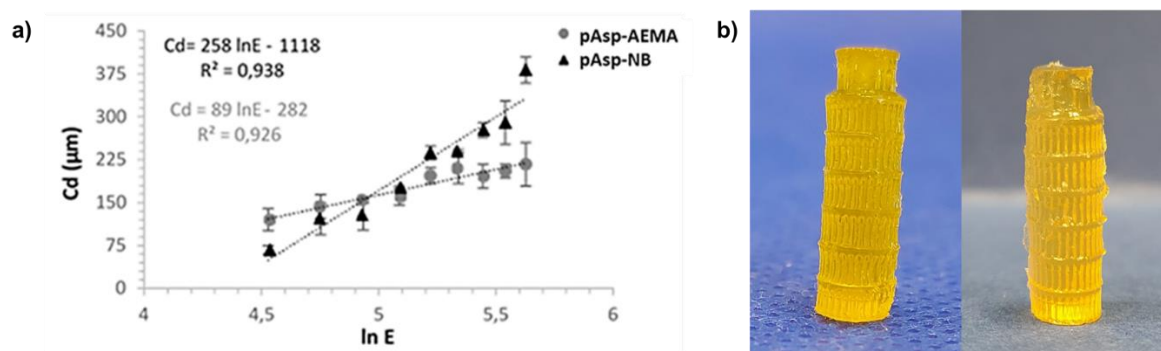


Figure 3. (a) Working curves of the DLP formulations exposed to 405 nm and 23.16 mW cm^{-2} . C_d represents the thickness of the cured resin and $\ln E$ the natural logarithm of the energy applied to the resin. The slope of the fitting equation represents the polymerization depth (D_p) and the value of E for zero-thickness represents the critical curing dose, (b) Pictures of the "Pisa Tower" structures obtained by DLP for pAsp-AEMA (left) and pAsp-NB (right).

3.4.2. 2PP

A proof-of-concept towards the processability of the materials by 2PP was shown by a structuring performance experiment as previously reported by Van Hoorick *et al.* for gelatin-based formulations [31, 60]. By scanning the laser beam through a formulation containing a suitable photo-initiator, polymerization can occur in a narrow focal point due to the simultaneous absorption of two photons by the photo-initiator. Hence, radicals are generated inducing crosslinking of the material in a narrow region. In this way, complex 3D hydrogel structures with high precision can be made by scanning the laser beam through the formulation according to a CAD design, followed by a washing step to remove the non-crosslinked material [60]. In the 2PP structuring performance experiment, $100 \times 100 \times 100 \mu\text{m}^3$ cubes were printed in a droplet of the precursor solutions on top of a silanized glass slide with a constant scanning speed of 600 mm s^{-1} and a varying average laser power, to determine the minimal power needed to obtain crosslinking. The precursor solutions contained 30 w/v% of pAsp-AEMA or pAsp-NB (with 0.50 eq. DTT) and 1 mM of the water-soluble and highly efficient 2PP photo-initiator P2CK in PBS [64]. For the pAsp-NB based precursor solution, an array of cubes was written in the droplet by variation of the laser power between 5 and 100 mW in increments of 5 mW. The 2PP threshold to obtain crosslinking for this formulation was 45 mW. For pAsp-AEMA, the laser power was varied between 100 and 250 mW in increments of 10 mW. Here, the threshold value was 140 mW, which was much higher than observed for pAsp-NB. These results show that both materials are processable via 2PP, but that there is a difference in processing performance since the pAsp-NB resin requires much lower laser power to produce structures than an equally concentrated pAsp-AEMA resin. However, these results were anticipated as the thiol-ene step-growth crosslinking has a much lower initiation threshold and exhibits faster reaction kinetics compared to chain-growth crosslinking, which was also observed before for photo-crosslinkable gelatin [30, 31, 34].

Finally, the potential to manufacture more complicated structures was demonstrated by 2PP printing of the two resins according to a CAD design of a snowflake with dimensions of $200 \mu\text{m} \times 180 \mu\text{m} \times 100 \mu\text{m}$ (**Figure 4a**). For the resin containing 30 w/v% pAsp-NB and 0.50 eq. DTT, the structure was printed with a laser power of 100 mW, as the laser power is usually set to double the threshold value to obtain well-defined structures [72]. The printing speed was reduced to 100 mm s^{-1} to obtain a better CAD-CAM mimicry. In **Figure 4b**, optical and confocal microscopy pictures of the obtained structure are shown. The dimensions of the obtained structure were determined through analysis of the optical microscopy pictures. The print showed a high precision, but the dimensions in the x and y direction were larger than the targeted dimensions of the CAD design, since the structures were visualized in their swollen form. Furthermore, confocal microscopy showed the 3D nature of the printed structure and the excellent CAD-CAM mimicry. For the resin based on 30 w/v% pAsp-AEMA, a laser power of 300 mW and a scanning speed of 300 mm s^{-1} were employed. The structure was also observed in its swollen form (**Figure 4c**). This print showed an excellent CAD-CAM mimicry and the shape could be clearly identified. When the two structures are compared, it can be observed that the structure made from crosslinked pAsp-AEMA

shows less extensive swelling than the structure from crosslinked pAsp-NB, which was already observed during the swelling experiments with hydrogel sheets made from both materials.

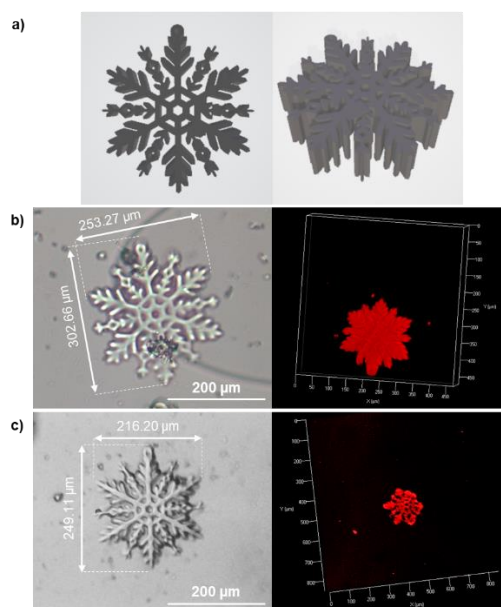


Figure 4. (a) CAD design used to print a snowflake ($x = 200 \mu\text{m}$, $y = 180 \mu\text{m}$ and $z = 100 \mu\text{m}$), (b) optical microscopy (left) and confocal microscopy (right) images of the structures obtained from a 30 w/v% pAsp-NB resin with 0.50 eq. DTT and 1 mM P2CK in PBS via 2PP exploiting a laser power of 100 mW and a scanning speed of 100 mm s^{-1} , (c) optical microscopy (left) and confocal microscopy (right) images of the structures obtained exploiting a 30 w/v% pAsp-AEMA resin with 1 mM P2CK in PBS via 2PP with a laser power of 300 mW and a scanning speed of 300 mm s^{-1} . Microscope images of all structures were taken in their swollen form.

4. Conclusion

In the present work, two types of modified pAsp derivatives were synthesized. Depending on the functional group that was incorporated (NB or AEMA), crosslinking occurred via a different mechanism, namely a thiol-ene step-growth mechanism or a chain-growth mechanism. *In situ* photo-rheology measurements showed that both derivatives were photo-crosslinkable and that the mechanism had an influence on the crosslinking kinetics and on the final mechanical stiffness of the formed networks. pAsp-NB showed faster crosslinking kinetics, while the post-polymerization G' was $29.4 \pm 1.3 \text{ kPa}$ compared to $135.1 \pm 4.7 \text{ kPa}$ for pAsp-AEMA, and hence pAsp-AEMA hydrogels exhibited a higher stiffness. The crosslinking mechanism also had an influence on the final network topology, which was indicated by a higher swelling ratio for pAsp-NB compared to pAsp-AEMA ($45.7 \pm 2.0 \text{ g g}^{-1}$ compared to $7.4 \pm 0.2 \text{ g g}^{-1}$). Furthermore, a difference in gel fraction was observed between pAsp-NB ($75.9 \pm 2.8\%$) and pAsp-AEMA ($87.8 \pm 4.2\%$). These results indicate more efficient network formation for pAsp-AEMA and the formation of a denser network for pAsp-AEMA compared to pAsp-NB. Finally, the mass swelling ratio and gel fraction was highly influenced by the photo-initiator and crosslinker concentration. An indirect Alamar Blue assay using HEK 293T cells as a model system confirmed that the synthesized hydrogels were not cytotoxic. Both pAsp-NB and pAsp-AEMA allowed cell growth, proving the absence of leachables in toxic concentrations in the hydrogels after sterilization and washing with EtOH.

Finally, a proof-of-concept was provided for processing the developed hydrogels by means of DLP and 2PP. A good CAD-CAM mimicry was obtained for both materials in DLP, with a superior outcome for

pAsp-AEMA. The possibility to print complex structures of the materials with excellent CAD-CAM mimicry was also proven for 2PP by printing a snowflake structure. Hence, we developed photo-crosslinkable pAsp-derivatives which are compatible with light-based AM techniques and which showed no cytotoxicity, paving the way towards unprecedented processing capabilities for pAsp serving biomedical applications.

Acknowledgements

Project 'GREENER' was financed within the Interreg V program Flanders-the Netherlands, a cross-border consortium with financial support of the European Fund for Regional Development with co-financing of the province East-Flanders and the Ministry of Economic Affairs and Climate (the Netherlands). Furthermore, the authors would like to thank Lana Van Damme for acquiring the confocal microscopy images and Sofiya Vynnytska for the GPC measurements in DMF.

Data availability

The raw/processed data required to reproduce these findings cannot be shared at this time due to technical or time limitations. Data will be made available on request.

References

- [1] Meka, V. S.; Sing, M. K. G.; Pichika, M. R.; Nali, S. R.; Kolapalli, V. R. M.; Kesharwani, P. A. Comprehensive Review on Polyelectrolyte Complexes. *Drug Discov. Today*, **2017**, *22* (11), 1697–1706. <https://doi.org/10.1016/j.drudis.2017.06.008>.
- [2] Alford, D. D.; Wheeler, A. P.; Pettigrew, C. A. Biodegradation of Thermally Synthesized Polyaspartate. *J. Environ. Polym. Degrad.*, **1994**, *2* (4), 225–236. <https://doi.org/10.1007/BF02071970>.
- [3] Tabata, K.; Kajiyama, M.; Hiraishi, T.; Abe, H.; Yamato, I.; Doi, Y. Purification and Characterization of Poly(Aspartic Acid) Hydrolase from *Sphingomonas* Sp. KT-1. *Biomacromolecules*, **2001**, *2* (4), 1155–1160. <https://doi.org/10.1021/bm0155468>.
- [4] Adelnia, H.; Tran, H. D. N.; Little, P. J.; Blakey, I.; Ta, H. T. Poly(Aspartic Acid) in Biomedical Applications: From Polymerization, Modification, Properties, Degradation, and Biocompatibility to Applications. *ACS Biomater. Sci. Eng.*, **2021**, *7* (6), 2083–2105. <https://doi.org/10.1021/acsbiomaterials.1c00150>.
- [5] Thombre, S. M.; Sarwade, B. D. Synthesis and Biodegradability of Polyaspartic Acid: A Critical Review. *J. Macromol. Sci. Part A*, **2005**, *42* (9), 1299–1315. <https://doi.org/10.1080/10601320500189604>.
- [6] Sharma, S.; Dua, A.; Malik, A. Polyaspartic Acid Based Superabsorbent Polymers. *Eur. Polym. J.*, **2014**, *59*, 363–376. <https://doi.org/10.1016/j.eurpolymj.2014.07.043>.
- [7] Adelnia, H.; Blakey, I.; Little, P. J.; Ta, H. T. Hydrogels Based on Poly(Aspartic Acid): Synthesis and Applications. *Front. Chem.*, **2019**, *7*. <https://doi.org/10.3389/fchem.2019.00755>.
- [8] Jalalvandi, E.; Shavandi, A. Polysuccinimide and Its Derivatives: Degradable and Water Soluble Polymers (Review). *Eur. Polym. J.*, **2018**, *109*, 43–54. <https://doi.org/10.1016/j.eurpolymj.2018.08.056>.
- [9] Xu, M.; Zhao, Y.; Feng, M. Polyaspartamide Derivative Nanoparticles with Tunable Surface Charge Achieve Highly Efficient Cellular Uptake and Low Cytotoxicity. *Langmuir*, **2012**, *28* (31), 11310–11318. <https://doi.org/10.1021/la3025028>.
- [10] Fu, Y.-C.; Fu, T.-F.; Wang, H.-J.; Lin, C.-W.; Lee, G.-H.; Wu, S.-C.; Wang, C.-K. Aspartic Acid-

- Based Modified PLGA–PEG Nanoparticles for Bone Targeting: In Vitro and in Vivo Evaluation. *Acta Biomater.*, **2014**, *10* (11), 4583–4596. <https://doi.org/10.1016/j.actbio.2014.07.015>.
- [11] Dou, X. B.; Hu, Y.; Zhao, N. N.; Xu, F. J. Different Types of Degradable Vectors from Low-Molecular-Weight Polycation-Functionalized Poly(Aspartic Acid) for Efficient Gene Delivery. *Biomaterials*, **2014**, *35* (9), 3015–3026. <https://doi.org/10.1016/j.biomaterials.2013.12.017>.
- [12] Juriga, D.; Nagy, K.; Jedlovszky-Hajdú, A.; Perczel-Kovách, K.; Chen, Y. M.; Varga, G.; Zrínyi, M. Biodegradation and Osteosarcoma Cell Cultivation on Poly(Aspartic Acid) Based Hydrogels. *ACS Appl. Mater. Interfaces*, **2016**, *8* (36), 23463–23476. <https://doi.org/10.1021/acsami.6b06489>.
- [13] Yavvari, P. S.; Awasthi, A. K.; Sharma, A.; Bajaj, A.; Srivastava, A. Emerging Biomedical Applications of Polyaspartic Acid-Derived Biodegradable Polyelectrolytes and Polyelectrolyte Complexes. *J. Mater. Chem. B*, **2019**, *7* (13), 2102–2122. <https://doi.org/10.1039/C8TB02962H>.
- [14] Fang, L.; Zhao, Y.; Tan, T. W. Preparation and Water Absorbent Behavior of Superabsorbent Polyaspartic Acid Resin. *J. Polym. Res.*, **2006**, *13* (2), 145–152. <https://doi.org/10.1007/s10965-005-9022-x>.
- [15] Gyenes, T.; Torma, V.; Gyarmati, B.; Zrínyi, M. Synthesis and Swelling Properties of Novel PH-Sensitive Poly(Aspartic Acid) Gels. *Acta Biomater.*, **2008**, *4* (3), 733–744. <https://doi.org/10.1016/j.actbio.2007.12.004>.
- [16] Gyarmati, B.; Mészár, E. Z.; Kiss, L.; Deli, M. A.; László, K.; Szilágyi, A. Supermacroporous Chemically Cross-Linked Poly(Aspartic Acid) Hydrogels. *Acta Biomater.*, **2015**, *22*, 32–38. <https://doi.org/10.1016/j.actbio.2015.04.033>.
- [17] Zhang, C.; Wu, S.; Wu, J.; Wu, D.; Qin, X. Preparation and Characterization of Microporous Sodium Poly(Aspartic Acid) Nanofibrous Hydrogel. *J. Porous Mater.*, **2017**, *24* (1), 75–84. <https://doi.org/10.1007/s10934-016-0239-3>.
- [18] Qiao, L.; Liu, C.; Liu, C.; Hu, F.; Li, X.; Wang, C.; Jian, X. Study on New Polymer Crosslinking Agents and Their Functional Hydrogels. *Eur. Polym. J.*, **2020**, *134*, 109835. <https://doi.org/10.1016/j.eurpolymj.2020.109835>.
- [19] Jedlovszky-Hajdu, A.; Molnar, K.; Nagy, P. M.; Sinko, K.; Zrínyi, M. Preparation and Properties of a Magnetic Field Responsive Three-Dimensional Electrospun Polymer Scaffold. *Colloids Surfaces A Physicochem. Eng. Asp.*, **2016**, *503*, 79–87. <https://doi.org/10.1016/j.colsurfa.2016.05.036>.
- [20] Szilágyi, B. Á.; Gyarmati, B.; Horvát, G.; Laki, Á.; Budai-Szűcs, M.; Csányi, E.; Sandri, G.; Bonferoni, M. C.; Szilágyi, A. The Effect of Thiol Content on the Gelation and Mucoadhesion of Thiolated Poly(Aspartic Acid). *Polym. Int.*, **2017**, *66* (11), 1538–1545. <https://doi.org/10.1002/pi.5411>.
- [21] Gyarmati, B.; Némethy, Á.; Szilágyi, A. Reversible Response of Poly(Aspartic Acid) Hydrogels to External Redox and PH Stimuli. *RSC Adv.*, **2014**, *4* (17), 8764. <https://doi.org/10.1039/c3ra47530a>.
- [22] Krisch, E.; Gyarmati, B.; Barczikai, D.; Lapeyre, V.; Szilágyi, B. Á.; Ravaine, V.; Szilágyi, A. Poly(Aspartic Acid) Hydrogels Showing Reversible Volume Change upon Redox Stimulus. *Eur. Polym. J.*, **2018**, *105*, 459–468. <https://doi.org/10.1016/j.eurpolymj.2018.06.011>.
- [23] Zrínyi, M.; Gyenes, T.; Juriga, D.; Kim, J.-H. Volume Change of Double Cross-Linked Poly(Aspartic Acid) Hydrogels Induced by Cleavage of One of the Crosslinks. *Acta Biomater.*, **2013**, *9* (2), 5122–5131. <https://doi.org/10.1016/j.actbio.2012.08.046>.
- [24] Budai-Szűcs, M.; Horvát, G.; Gyarmati, B.; Szilágyi, B. Á.; Szilágyi, A.; Csihi, T.; Berkó, S.; Szabó-Révész, P.; Mori, M.; Sandri, G.; et al. In Vitro Testing of Thiolated Poly(Aspartic Acid) from Ophthalmic Formulation Aspects. *Drug Dev. Ind. Pharm.*, **2016**, *42* (8), 1241–1246. <https://doi.org/10.3109/03639045.2015.1118497>.
- [25] Horvát, G.; Gyarmati, B.; Berkó, S.; Szabó-Révész, P.; Szilágyi, B. Á.; Szilágyi, A.; Soós, J.; Sandri, G.; Bonferoni, M. C.; Rossi, S.; et al. Thiolated Poly(Aspartic Acid) as Potential in Situ

- Gelling, Ocular Mucoadhesive Drug Delivery System. *Eur. J. Pharm. Sci.*, **2015**, *67*, 1–11. <https://doi.org/10.1016/j.ejps.2014.10.013>.
- [26] Duggan, S.; Cummins, W.; O' Donovan, O.; Hughes, H.; Owens, E. Thiolated Polymers as Mucoadhesive Drug Delivery Systems. *Eur. J. Pharm. Sci.*, **2017**, *100*, 64–78. <https://doi.org/10.1016/j.ejps.2017.01.008>.
- [27] Krisch, E.; Messenger, L.; Gyarmati, B.; Ravaine, V.; Szilágyi, A. Redox- and PH-Responsive Nanogels Based on Thiolated Poly(Aspartic Acid). *Macromol. Mater. Eng.*, **2016**, *301* (3), 260–266. <https://doi.org/10.1002/mame.201500119>.
- [28] De Grave, L.; Tenório Filho, J. R.; Snoeck, D.; Vynnytska, S.; De Belie, N.; Bernaerts, K. V.; Van Vlierberghe, S. Poly(Aspartic Acid) Superabsorbent Polymers as Biobased and Biodegradable Additives for Self-Sealing of Cementitious Mortar. *J. Sustain. Cem. Mater.*, **2022**, 1–16. <https://doi.org/10.1080/21650373.2022.2137861>.
- [29] Yu, C.; Schimelman, J.; Wang, P.; Miller, K. L.; Ma, X.; You, S.; Guan, J.; Sun, B.; Zhu, W.; Chen, S. Photopolymerizable Biomaterials and Light-Based 3D Printing Strategies for Biomedical Applications. *Chem. Rev.*, **2020**, *120* (19), 10695–10743. <https://doi.org/10.1021/acs.chemrev.9b00810>.
- [30] Van Hoorick, J.; Tytgat, L.; Dobos, A.; Ottevaere, H.; Van Erps, J.; Thienpont, H.; Ovsianikov, A.; Dubruel, P.; Van Vlierberghe, S. (Photo-)Crosslinkable Gelatin Derivatives for Biofabrication Applications. *Acta Biomater.*, **2019**, *97*, 46–73. <https://doi.org/10.1016/j.actbio.2019.07.035>.
- [31] Van Hoorick, J.; Gruber, P.; Markovic, M.; Rollot, M.; Graulus, G.-J.; Vagenende, M.; Tromayer, M.; Van Erps, J.; Thienpont, H.; Martins, J. C.; et al. Highly Reactive Thiol-Norbornene Photo-Click Hydrogels: Toward Improved Processability. *Macromol. Rapid Commun.*, **2018**, *39* (14), 1800181–1800187. <https://doi.org/10.1002/marc.201800181>.
- [32] Van Den Bulcke, A. I.; Bogdanov, B.; De Rooze, N.; Schacht, E. H.; Cornelissen, M.; Berghmans, H. Structural and Rheological Properties of Methacrylamide Modified Gelatin Hydrogels. *Biomacromolecules*, **2000**, *1* (1), 31–38. <https://doi.org/10.1021/bm990017d>.
- [33] Tytgat, L.; Van Damme, L.; Van Hoorick, J.; Declercq, H.; Thienpont, H.; Ottevaere, H.; Blondeel, P.; Dubruel, P.; Van Vlierberghe, S. Additive Manufacturing of Photo-Crosslinked Gelatin Scaffolds for Adipose Tissue Engineering. *Acta Biomater.*, **2019**, *94*, 340–350. <https://doi.org/10.1016/j.actbio.2019.05.062>.
- [34] Tytgat, L.; Dobos, A.; Markovic, M.; Van Damme, L.; Van Hoorick, J.; Bray, F.; Thienpont, H.; Ottevaere, H.; Dubruel, P.; Ovsianikov, A.; et al. High-Resolution 3D Bioprinting of Photo-Cross-Linkable Recombinant Collagen to Serve Tissue Engineering Applications. *Biomacromolecules*, **2020**, *21* (10), 3997–4007. <https://doi.org/10.1021/acs.biomac.0c00386>.
- [35] Pien, N.; Pezzoli, D.; Van Hoorick, J.; Copes, F.; Vansteenland, M.; Albu, M.; De Meulenaer, B.; Mantovani, D.; Van Vlierberghe, S.; Dubruel, P. Development of Photo-Crosslinkable Collagen Hydrogel Building Blocks for Vascular Tissue Engineering Applications: A Superior Alternative to Methacrylated Gelatin? *Mater. Sci. Eng. C*, **2021**, *130*, 112460. <https://doi.org/10.1016/j.msec.2021.112460>.
- [36] Parenteau-Bareil, R.; Gauvin, R.; Berthod, F. Collagen-Based Biomaterials for Tissue Engineering Applications. *Materials (Basel)*, **2010**, *3* (3), 1863–1887. <https://doi.org/10.3390/ma3031863>.
- [37] Xu, X.; Jha, A. K.; Harrington, D. A.; Farach-Carson, M. C.; Jia, X. Hyaluronic Acid-Based Hydrogels: From a Natural Polysaccharide to Complex Networks. *Soft Matter*, **2012**, *8* (12), 3280. <https://doi.org/10.1039/c2sm06463d>.
- [38] Graulus, G.-J.; Mignon, A.; Van Vlierberghe, S.; Declercq, H.; Fehér, K.; Cornelissen, M.; Martins, J. C.; Dubruel, P. Cross-Linkable Alginate-Graft-Gelatin Copolymers for Tissue Engineering Applications. *Eur. Polym. J.*, **2015**, *72*, 494–506. <https://doi.org/10.1016/j.eurpolymj.2015.06.033>.
- [39] Jeon, O.; Bouhadir, K. H.; Mansour, J. M.; Alsberg, E. Photocrosslinked Alginate Hydrogels with Tunable Biodegradation Rates and Mechanical Properties. *Biomaterials*, **2009**, *30* (14), 2724–

2734. <https://doi.org/10.1016/j.biomaterials.2009.01.034>.
- [40] Chou, A. I.; Nicoll, S. B. Characterization of Photocrosslinked Alginate Hydrogels for Nucleus Pulposus Cell Encapsulation. *J. Biomed. Mater. Res. Part A*, **2009**, *91A* (1), 187–194. <https://doi.org/10.1002/jbm.a.32191>.
- [41] Skardal, A.; Zhang, J.; Prestwich, G. D. Bioprinting Vessel-like Constructs Using Hyaluronan Hydrogels Crosslinked with Tetrahedral Polyethylene Glycol Tetracrylates. *Biomaterials*, **2010**, *31* (24), 6173–6181. <https://doi.org/10.1016/j.biomaterials.2010.04.045>.
- [42] Warner, J.; Soman, P.; Zhu, W.; Tom, M.; Chen, S. Design and 3D Printing of Hydrogel Scaffolds with Fractal Geometries. *ACS Biomater. Sci. Eng.*, **2016**, *2* (10), 1763–1770. <https://doi.org/10.1021/acsbomaterials.6b00140>.
- [43] Thijssen, Q.; Parmentier, L.; Augustyniak, E.; Mouthuy, P.; Van Vlierberghe, S. From Chain Growth to Step Growth Polymerization of Photoreactive Poly- ϵ -Caprolactone: The Network Topology of Bioresorbable Networks as Tool in Tissue Engineering. *Adv. Funct. Mater.*, **2022**, *32* (20), 2108869. <https://doi.org/10.1002/adfm.202108869>.
- [44] Wang, Y.; Zhang, S.; Wang, J. Photo-Crosslinkable Hydrogel and Its Biological Applications. *Chinese Chem. Lett.*, **2021**, *32* (5), 1603–1614. <https://doi.org/10.1016/j.cclet.2020.11.073>.
- [45] Muir, V. G.; Burdick, J. A. Chemically Modified Biopolymers for the Formation of Biomedical Hydrogels. *Chem. Rev.*, **2021**, *121* (18), 10908–10949. <https://doi.org/10.1021/acs.chemrev.0c00923>.
- [46] Colombani, D. Chain-Growth Control in Free Radical Polymerization. *Prog. Polym. Sci.*, **1997**, *22* (8), 1649–1720. [https://doi.org/10.1016/S0079-6700\(97\)00022-1](https://doi.org/10.1016/S0079-6700(97)00022-1).
- [47] Ding, F.-C.; Hsu, S.; Chiang, W.-Y. Synthesis of a New Photoreactive Gelatin with BTDA and HEMA Derivatives. *J. Appl. Polym. Sci.*, **2008**, *109* (1), 589–596. <https://doi.org/10.1002/app.28025>.
- [48] Seiffert, S. Origin of Nanostructural Inhomogeneity in Polymer-Network Gels. *Polym. Chem.*, **2017**, *8* (31), 4472–4487. <https://doi.org/10.1039/C7PY01035D>.
- [49] Lim, K. S.; Schon, B. S.; Mekhileri, N. V.; Brown, G. C. J.; Chia, C. M.; Prabakar, S.; Hooper, G. J.; Woodfield, T. B. F. New Visible-Light Photoinitiating System for Improved Print Fidelity in Gelatin-Based Bioinks. *ACS Biomater. Sci. Eng.*, **2016**, *2* (10), 1752–1762. <https://doi.org/10.1021/acsbomaterials.6b00149>.
- [50] Yilmaz, G.; Yagci, Y. Light-Induced Step-Growth Polymerization. *Prog. Polym. Sci.*, **2020**, *100*, 101178. <https://doi.org/10.1016/j.progpolymsci.2019.101178>.
- [51] Kolb, H. C.; Finn, M. G.; Sharpless, K. B. Click Chemistry: Diverse Chemical Function from a Few Good Reactions. *Angew. Chemie Int. Ed.*, **2001**, *40* (11), 2004–2021. [https://doi.org/10.1002/1521-3773\(20010601\)40:11<2004::AID-ANIE2004>3.0.CO;2-5](https://doi.org/10.1002/1521-3773(20010601)40:11<2004::AID-ANIE2004>3.0.CO;2-5).
- [52] Machado, T. O.; Sayer, C.; Araujo, P. H. H. Thiol-Ene Polymerisation: A Promising Technique to Obtain Novel Biomaterials. *Eur. Polym. J.*, **2017**, *86*, 200–215. <https://doi.org/10.1016/j.eurpolymj.2016.02.025>.
- [53] Hoyle, C. E.; Bowman, C. N. Thiol-Ene Click Chemistry. *Angew. Chemie Int. Ed.*, **2010**, *49* (9), 1540–1573. <https://doi.org/10.1002/anie.200903924>.
- [54] Hoyle, C. E.; Lee, T. Y.; Roper, T. Thiol-Ene: Chemistry of the Past with Promise for the Future. *J. Polym. Sci. Part A Polym. Chem.*, **2004**, *42* (21), 5301–5338. <https://doi.org/10.1002/pola.20366>.
- [55] Lin, C.-C.; Ki, C. S.; Shih, H. Thiol-Norbornene Photoclick Hydrogels for Tissue Engineering Applications. *J. Appl. Polym. Sci.*, **2015**, *132* (8), 41563–41573. <https://doi.org/10.1002/app.41563>.
- [56] Hoch, E.; Schuh, C.; Hirth, T.; Tovar, G. E. M.; Borchers, K. Stiff Gelatin Hydrogels Can Be Photo-Chemically Synthesized from Low Viscous Gelatin Solutions Using Molecularly Functionalized Gelatin with a High Degree of Methacrylation. *J. Mater. Sci. Mater. Med.*, **2012**,

- 23 (11), 2607–2617. <https://doi.org/10.1007/s10856-012-4731-2>.
- [57] Bertlein, S.; Brown, G.; Lim, K. S.; Jungst, T.; Boeck, T.; Blunk, T.; Tessmar, J.; Hooper, G. J.; Woodfield, T. B. F.; Groll, J. Thiol-Ene Clickable Gelatin: A Platform Bioink for Multiple 3D Biofabrication Technologies. *Adv. Mater.*, **2017**, *29* (44), 1703404. <https://doi.org/10.1002/adma.201703404>.
- [58] Goethals, F.; Frank, D.; Du Prez, F. Protected Thiol Strategies in Macromolecular Design. *Prog. Polym. Sci.*, **2017**, *64*, 76–113. <https://doi.org/10.1016/j.progpolymsci.2016.09.003>.
- [59] Markovic, M.; Van Hoorick, J.; Hözl, K.; Tromayer, M.; Gruber, P.; Nürnberger, S.; Dubruel, P.; Van Vlierberghe, S.; Liska, R.; Ovsianikov, A. Hybrid Tissue Engineering Scaffolds by Combination of Three-Dimensional Printing and Cell Photoencapsulation. *J. Nanotechnol. Eng. Med.*, **2015**, *6* (2), 210011–210017. <https://doi.org/10.1115/1.4031466>.
- [60] Van Hoorick, J.; Gruber, P.; Markovic, M.; Tromayer, M.; Van Erps, J.; Thienpont, H.; Liska, R.; Ovsianikov, A.; Dubruel, P.; Van Vlierberghe, S. Cross-Linkable Gelatins with Superior Mechanical Properties Through Carboxylic Acid Modification: Increasing the Two-Photon Polymerization Potential. *Biomacromolecules*, **2017**, *18* (10), 3260–3272. <https://doi.org/10.1021/acs.biomac.7b00905>.
- [61] Chaudhary, R.; Fabbri, P.; Leoni, E.; Mazzanti, F.; Akbari, R.; Antonini, C. Additive Manufacturing by Digital Light Processing: A Review. *Prog. Addit. Manuf.*, **2022**. <https://doi.org/10.1007/s40964-022-00336-0>.
- [62] Bennett, J. Measuring UV Curing Parameters of Commercial Photopolymers Used in Additive Manufacturing. *Addit. Manuf.*, **2017**, *18*, 203–212. <https://doi.org/10.1016/j.addma.2017.10.009>.
- [63] Jacobs, P. F.; Reid, D. T.; SME., C. and A. S. A. of. *Rapid Prototyping & Manufacturing: Fundamentals of Stereolithography*; Society of Manufacturing Engineers, 1992.
- [64] Dobos, A.; Steiger, W.; Theiner, D.; Gruber, P.; Lunzer, M.; Van Hoorick, J.; Van Vlierberghe, S.; Ovsianikov, A. Screening of Two-Photon Activated Photodynamic Therapy Sensitizers Using a 3D Osteosarcoma Model. *Analyst*, **2019**, *144* (9), 3056–3063. <https://doi.org/10.1039/C9AN00068B>.
- [65] Muller, R.; Gerard, E.; Dugand, P.; Rempp, P.; Gnanou, Y. Rheological Characterization of the Gel Point: A New Interpretation. *Macromolecules*, **1991**, *24* (6), 1321–1326. <https://doi.org/10.1021/ma00006a017>.
- [66] Van Hoorick, J.; Dobos, A.; Markovic, M.; Gheysens, T.; Van Damme, L.; Gruber, P.; Tytgat, L.; Van Erps, J.; Thienpont, H.; Dubruel, P.; et al. Thiol-Norbornene Gelatin Hydrogels: Influence of Thiolated Crosslinker on Network Properties and High Definition 3D Printing. *Biofabrication*, **2021**, *13* (1), 015017. <https://doi.org/10.1088/1758-5090/abc95f>.
- [67] Van Damme, L.; Van Hoorick, J.; Blondeel, P.; Van Vlierberghe, S. Toward Adipose Tissue Engineering Using Thiol-Norbornene Photo-Crosslinkable Gelatin Hydrogels. *Biomacromolecules*, **2021**, *22* (6), 2408–2418. <https://doi.org/10.1021/acs.biomac.1c00189>.
- [68] Di Lorenzo, F.; Seiffert, S. Nanostructural Heterogeneity in Polymer Networks and Gels. *Polym. Chem.*, **2015**, *6* (31), 5515–5528. <https://doi.org/10.1039/C4PY01677G>.
- [69] Dobos, A.; Van Hoorick, J.; Steiger, W.; Gruber, P.; Markovic, M.; Andriotis, O. G.; Rohatschek, A.; Dubruel, P.; Thurner, P. J.; Van Vlierberghe, S.; et al. Thiol–Gelatin–Norbornene Bioink for Laser-Based High-Definition Bioprinting. *Adv. Healthc. Mater.*, **2020**, *9* (15), 1900752. <https://doi.org/10.1002/adhm.201900752>.
- [70] Kadry, H.; Wadnap, S.; Xu, C.; Ahsan, F. Digital Light Processing (DLP) 3D-Printing Technology and Photoreactive Polymers in Fabrication of Modified-Release Tablets. *Eur. J. Pharm. Sci.*, **2019**, *135*, 60–67. <https://doi.org/10.1016/j.ejps.2019.05.008>.
- [71] Arias-Ferreiro, G.; Ares-Pernas, A.; Lasagabáster-Latorre, A.; Aranburu, N.; Guerrica-Echevarria, G.; Dopico-García, M. S.; Abad, M.-J. Printability Study of a Conductive Polyaniline/Acrylic Formulation for 3D Printing. *Polymers (Basel)*, **2021**, *13* (13), 2068. <https://doi.org/10.3390/polym13132068>.

- [72] Zhou, X.; Hou, Y.; Lin, J. A Review on the Processing Accuracy of Two-Photon Polymerization. *AIP Adv.*, **2015**, 5 (3), 030701. <https://doi.org/10.1063/1.4916886>.